

# Effect of Permittivity and Permeability of a Flexible Magnetic Composite Material on the Performance and Miniaturization Capability of Planar Antennas for RFID and Wearable Wireless Applications

Lara J. Martin, *Member, IEEE*, Sooliam Ooi, *Senior Member, IEEE*, Daniela Staiculescu, *Member, IEEE*, Michael D. Hill, C. P. Wong, *Fellow, IEEE*, and Manos M. Tentzeris, *Senior Member, IEEE*

**Abstract**—This paper is an investigation of the feasibility of applying a mechanically flexible magnetic composite material to radio frequency identification (RFID) planar antennas operating in the lower ultrahigh-frequency (UHF) spectrum (~300–500 MHz). A key challenge is that the magnetic loss introduced by the magnetic composite must be sufficiently low for successful application at the targeted operating frequency. A flexible magnetic composite comprised of particles of Z-phase Co hexaferrite, also known as  $\text{Co}_2\text{Z}$ , in a silicone matrix was developed. To the authors' knowledge, this is the first flexible magnetic composite demonstrated to work at these frequencies. The benchmarking structure was a quarter-wavelength microstrip patch antenna. Antennas on the developed magnetic composite and pure silicone substrates were electromagnetically modeled in Ansoft High-Frequency Sounder System full wave electromagnetic software. A prototype of the antenna on the magnetic composite was fabricated, and good agreement between the simulated and measured results was found. Comparison of the antennas on the magnetic composite versus the pure silicone substrate showed miniaturization capability of 2.4 $\times$  and performance differences of increased bandwidth and reduced gain, both of which were attributed in part to the increase in the dielectric and magnetic losses. A key finding of this paper is that a small amount of permeability ( $\mu_r \sim 2.5$ ) can provide a substantial capability for miniaturization, while sufficiently low-magnetic loss can be introduced for successful application at the targeted operating frequency. This magnetic composite shows the capability to fulfill this balance and to be a feasible option for RFID,

flexible wearable, and conformal applications in the lower UHF spectrum.

**Index Terms**—Flexible structures, identification, magnetic materials, passive circuits, ultrahigh-frequency antennas.

## I. INTRODUCTION

**R**ADIO FREQUENCY identification (RFID) has enabled contactless transfer of information without the requirement of line of sight association, specifically between a reader and transponders that reside on an identified item. As the technology for RFID systems has developed, there has been a need to design more flexible systems enabled at the transponder, specifically the miniaturization of the transponder as well as ability to adjust the transponder mechanical form factor, adjust the read range, and tune system performance to accommodate electromagnetic (EM) absorption and interference from surrounding media [1] and [2]. 3-D transponder antennas that utilize wound coil inductors do make use of magnetic cores, but magnetic materials for 2-D embedded planar antennas have not yet been successfully realized for standard use. As their 3-D counterparts, 2-D embedded antennas can reap the same benefits from magnetic materials.

In many previous embedded inductor and antenna studies, it has been cited that the simultaneous objectives of miniaturization and improved performance are limited by the availability of materials that possess the required properties [3]–[5]. Studies on magnetic materials that may provide effective solutions and are compatible with currently established processing techniques and design requirements are needed for such materials to find their way into standard RFID antenna designs.

The capability for achieving miniaturization is demonstrated by the equation for the length of a quarter-wavelength microstrip antenna. The length of the quarter-wavelength microstrip antenna is  $\lambda/4$  as shown by (1) [6]

$$\frac{\lambda}{4} = \frac{c}{4f_r \sqrt{\mu_{eff} \epsilon_{eff}}} \quad (1)$$

Manuscript received April 11, 2008; revised June 29, 2009. Current version published November 20, 2009. Recommended for publication by Associate Editor J. J. Liu upon evaluation of reviewers' comments.

L. J. Martin is with Motorola, Plantation, FL 33322 USA (e-mail: lara.martin@motorola.com).

S. Ooi is with Blackberry Research and Development, Sunrise, FL 33323 USA (e-mail: sooi@rim.com).

D. Staiculescu is with the Athena Group, Georgia Institute of Technology, Atlanta, GA 30332 USA (e-mail: daniela@ece.gatech.edu).

M. D. Hill is with the Department of Research and Development, Trans-Tech, Adamstown, MD 21710 USA (e-mail: mike.hill@skyworksinc.com).

C. P. Wong is with the School of Materials Science and Engineering, Georgia Institute of Technology, Atlanta, GA 30332 USA (e-mail: cp.wong@mse.gatech.edu).

M. M. Tentzeris is with the School of Electrical and Computer Engineering, Georgia Institute of Technology, Atlanta, GA 30332 USA (e-mail: etentze@ece.gatech.edu).

Color versions of one or more of the figures in this paper are available online at <http://ieeexplore.ieee.org>.

Digital Object Identifier 10.1109/TCAPT.2009.2032767

where  $\lambda$  is wavelength,  $c$  is speed of light,  $f_r$  is resonant frequency,  $\mu_{eff}$  is effective permeability, and  $\epsilon_{eff}$  is effective permittivity. From (1), increasing permeability by the addition of a magnetic material to a quarter-wavelength microstrip antenna decreases the required length for resonance, enabling miniaturization. Further, the use of a magnetic material has been shown to increase the bandwidth and decrease the circuit  $Q$  as defined in (2) by the addition of some magnetic loss. However, only a limited increase in the magnetic loss can be tolerated for achieving successful microstrip designs [7]–[9]

$$Q = \frac{f_r}{BW}. \quad (2)$$

Only limited work has been done to use magnetic materials in microstrip antennas to achieve these benefits [6]–[10]. For microstrip antenna designs, increasing bandwidth and miniaturization are interdependent results that can work together for improved performance.

In this paper, the benchmark structure is a quarter-wavelength microstrip patch antenna in the lower ultrahigh-frequency (UHF) band ( $\sim 300$ – $500$  MHz) on both a flexible magnetic composite substrate and a pure silicone substrate. First, a flexible magnetic composite comprised of Z-phase Co hexaferrite, also known as  $\text{Co}_2\text{Z}$ , in a silicone matrix was developed and fabricated as a substrate for the antenna structure. Next, the material properties for the developed magnetic composite and the pure silicone substrates were determined. Then, EM simulation was applied to design two-microstrip patch antennas with identical operating frequencies, substrate thicknesses, and patch size:ground size ratios in order to compare the effects of the substrates. A prototype of the patch antenna on the flexible magnetic composite substrate was fabricated using standard printed circuit board processing techniques. Then, the simulated and measured results for the  $S_{11}$  parameter and 2-D radiation were obtained for determining the following antenna figures of merit: resonant frequency ( $f_r$ ), return loss ( $RL$ ), the  $-10$  dB bandwidth ( $-10$  dB  $BW$ ), the 2-D radiation patterns at  $\phi = 0^\circ$  and  $90^\circ$ , maximum gain, and circuit  $Q$  as defined by (2).

These figures of merit were compared and the capability for miniaturization was determined. The aim of this paper is to assess the difference in the antenna performance and miniaturization capability attributable to the developed flexible magnetic composite as well as the feasibility of applying the developed material to the lower UHF spectrum ( $\sim 300$ – $500$  MHz). To the authors' knowledge, this is the first flexible magnetic composite demonstrated to work at these frequencies.

## II. MATERIAL DEVELOPMENT

First, particles of Z-phase cobalt hexaferrite, as known as  $\text{Co}_2\text{Z}$ , were formulated.  $\text{Co}_2\text{Z}$  is a hexagonal ferrite, and the size distribution utilized in this paper was  $45$ – $150$   $\mu\text{m}$ . Then, a magnetic composite comprised of  $\text{Co}_2\text{Z}$  particles in a matrix of Dow Corning Sylgard 184 silicone was synthesized. Both the pure silicone and the developed magnetic composite were used as substrates for an antenna structure, in order to compare antenna performance and determine the capability for miniaturization.

The  $\text{Co}_2\text{Z}$  particles were synthesized by blending oxides and carbonates of the stoichiometric composition ( $\text{Ba}_3\text{Co}_2\text{Fe}_{24}\text{O}_{41}$ ) and heat treating in the range of  $1150$ – $1300$   $^\circ\text{C}$  to bring about the solid state reaction which forms single-phase  $\text{Co}_2\text{Z}$  material. Following the solid state reaction of the powder, the material was granulated, sintered above  $1200$   $^\circ\text{C}$ , and crushed to achieve the desired particle size. The magnetic composite was formulated by mixing 40 vol% ferrite particles in the uncured silicone to form a wet powder. To fabricate the substrate, the wet powder was transferred to a premade flat mold, constructed of 36-mm thick Cu foil sheet adhered with pure silicone to a bare 305 mm  $\times$  457 mm FR-4 laminate panel with a cutout in shape of the targeted substrate dimensions. Another 36-mm thick Cu foil sheet was then placed on top and more pure silicone was applied to the panel edges for adhesion. The final panel was then placed in a printed circuit board press and processed at  $121$   $^\circ\text{C}$  for 80 min. The silicone substrate was fabricated using the identical steps with the exception of using pure uncured silicone in the premade flat mold. Once the substrates were fabricated, a prototype antenna was made on the magnetic composite by standard double-sided printed circuit board processing techniques, which included drilling through-holes, plating the through-holes, patterning the copper, and routing to remove the resulting antenna from the panel.

The crystal structure of the  $\text{Co}_2\text{Z}$  particles was investigated by X-ray diffraction (XRD). The XRD was performed with a Philips 1830 XRD system with the PW3710 multipurpose diffractometer controller using Cu  $K_\alpha$  ( $\lambda = 0.1540562$  nm) radiation. Samples were prepared as powder with no attempt made to preferentially align the sample to obtain enhanced (001) reflections. The XRD pattern of the  $\text{Co}_2\text{Z}$  particles is shown in Fig. 1. All of the peaks in the pattern can be indexed to the Z-phase with no trace of the hexagonal M ( $\text{BaFe}_{12}\text{O}_{19}$ ) or Y ( $\text{Ba}_2\text{Co}_2\text{Fe}_{12}\text{O}_{22}$ ) phases present. M and Y phases form at lower temperatures and may leave a residue at the processing temperature if the blending is poor or the stoichiometry incorrect. If the conversion process is not taken to completion, small quantities of these earlier reactant phases can remain as impurities in the targeted final phase [11] and [12]. The X-ray pattern indicates that the conversion process to the Z-phase is complete to the resolution of the X-ray diffraction (between 1 and 2 volume percent). Single-phase material is important to minimize dielectric and magnetic loss as well as to obtain a stable dielectric constant and permeability over the targeted operating frequency range.

The material properties of the resulting magnetic composite silicone substrates were obtained to investigate the applicability to the targeted operating frequency, i.e., in the lower UHF band ( $\sim 300$ – $500$  MHz) and determine inputs for antenna design via EM simulation. The materials were measured using an HP4291A impedance analyzer to obtain complex permittivity ( $\epsilon^*$ ) and permeability ( $\mu^*$ ) (real and imaginary parts) with material fixtures 16453A for  $\epsilon^*$  and 16454A for  $\mu^*$  over the frequency range of 1 MHz to 1.8 GHz. There were five measurements taken for each  $\epsilon_r$ ,  $\mu_r$ ,  $\tan\delta_\epsilon$ , and  $\tan\delta_\mu$  to ensure repeatability.

Measuring the pure silicone substrate, it was determined that the material properties specified by the manufacturer

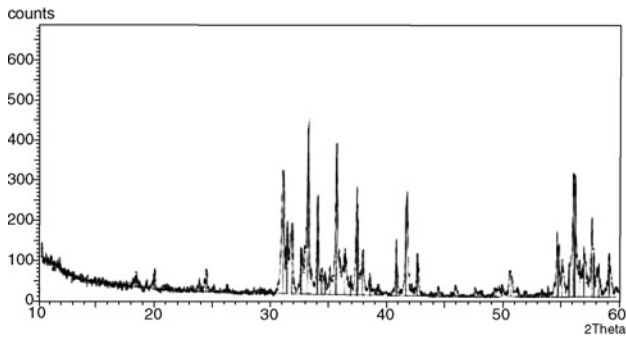
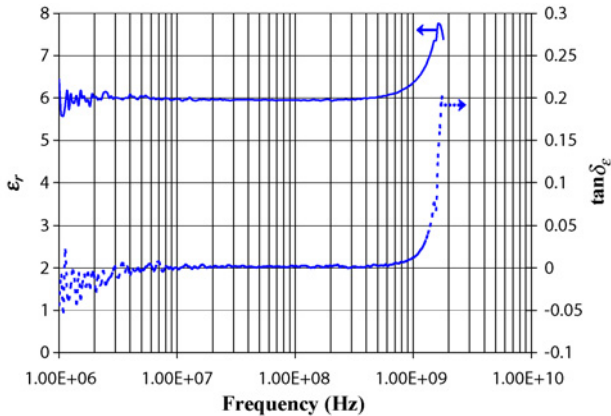
Fig. 1. XRD pattern of the  $\text{Co}_2\text{Z}$  particles.

TABLE I  
MATERIAL PROPERTIES FOR PURE SILICONE

$\epsilon_r$	2.65
$\tan\delta_\epsilon$	0.001
$\mu_r$	1
$\tan\delta_\mu$	0

Fig. 2. Permittivity as a function of frequency for the magnetic composite, including relative permittivity ( $\epsilon_r$ ) and dielectric loss tangent ( $\tan\delta_\epsilon$ ).

and shown in Table I were reasonable to use over the targeted operating frequencies. For the magnetic composite, the dispersive properties  $\epsilon_r$ ,  $\mu_r$ ,  $\tan\delta_\epsilon$ , and  $\tan\delta_\mu$  as a function of frequency were applied due to their variations over the targeted operating frequency range, particularly near the upper limit of their applicability at  $\sim 400$ – $500$  MHz. The values of  $\epsilon_r$ ,  $\mu_r$ ,  $\tan\delta_\epsilon$ , and  $\tan\delta_\mu$  obtained in single measurements are shown in Figs. 2 and 3. The form of the final material properties used was an 11-point moving average of the values shown in Figs. 2 and 3 in order to remove measurement artifacts and produce smoothed data, for better handling by EM simulation packages.

### III. ANTENNA DESIGN AND MEASUREMENT

The analyzed structure was a quarter-wavelength microstrip patch antenna in the lower UHF band ( $\sim 300$ – $500$  MHz). The approach was to apply the previously determined material properties  $\epsilon_r$ ,  $\mu_r$ ,  $\tan\delta_\epsilon$ , and  $\tan\delta_\mu$  and compare the patch antennas on the pure silicone versus the magnetic composite substrate. Table II shows the initial design rules for the patch

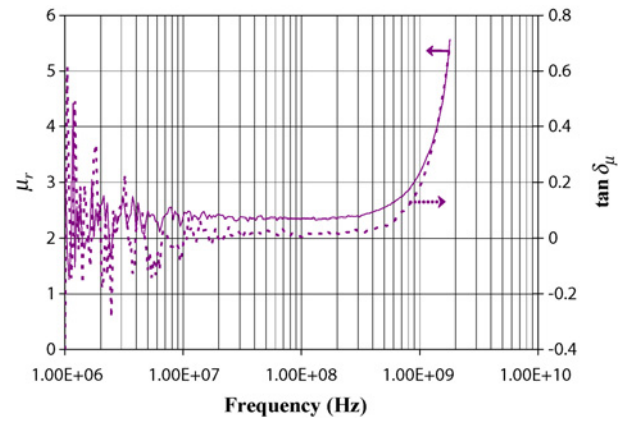
Fig. 3. Permeability as a function of frequency for the magnetic composite, including relative permeability ( $\mu_r$ ) and magnetic loss tangent ( $\tan\delta_\mu$ ).

TABLE II  
INITIAL DESIGN RULES FOR PATCH ANTENNAS

Operating Frequency	386 MHz
$h$ (Substrate Thickness)	3.2 mm
Patch Size:Ground Size	0.27

antennas, including targeted operating frequency, substrate thickness ( $h$ ), and the ratio of patch size to ground size.

For designing the analyzed antenna structures, Ansoft High-Frequency Sounder System (HFSS) version 11.0.1 simulation package, a full wave, finite element method EM solver, was applied. The material properties  $\epsilon_r$ ,  $\mu_r$ ,  $\tan\delta_\epsilon$ , and  $\tan\delta_\mu$  for the magnetic composite were inputted into the simulation as a function of frequency. The design methodology included first developing an isolated microstrip model on the substrate and then determining the microstrip width ( $w$ ) that gave characteristic impedance ( $Z_0$ ) of  $50\ \Omega$ . Then, the patch size was adjusted to tune to the targeted operating frequency. Finally, inset ( $d$ ) was adjusted to minimize return loss ( $RL$ ).

The patch antenna designs resulting from the EM simulations for the pure silicone and the magnetic composite substrate are shown in Figs. 4 and 5, respectively. The patch antenna design on the pure silicone substrate includes a microstrip feed to a  $115.6\ \text{mm}$  square patch over a  $425\ \text{mm}$  square ground and a path to short the patch to ground along the feed side. The patch antenna design on the magnetic composite substrate includes a microstrip feed to a  $49\ \text{mm}$  square patch over a  $180\ \text{mm}$  square ground and a path to short the patch to ground along the feed side. The patch on the magnetic composite is smaller (miniaturized) compared to the patch on pure silicone in order to achieve the common targeted operating frequency of  $386\ \text{MHz}$ . A prototype of the resulting patch antenna design for the magnetic composite was built and is shown in Fig. 6. For the prototype, the shorting of the patch to ground along the feed side was realized with through-holes having  $0.508\ \text{mm}$  diameter and a  $2.032\ \text{mm}$  pitch along the feed side.

The performance figures of merit for the patch antennas were  $f_r$ ,  $RL$ , the  $-10\ \text{dB BW}$ , the 2-D radiation patterns at  $\phi = 0^\circ$  and  $90^\circ$ , the maximum gain, and the  $Q$  as defined in (2). For the radiation patterns,  $\phi$  is defined as the angle

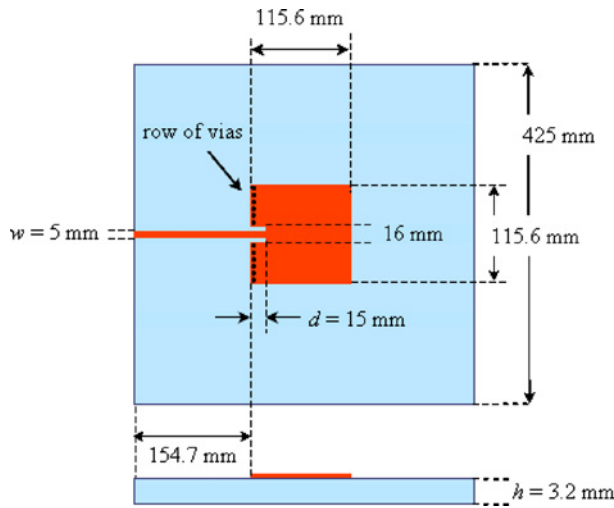


Fig. 4. Dimensions of patch antenna design on pure silicone substrate (not drawn to scale).

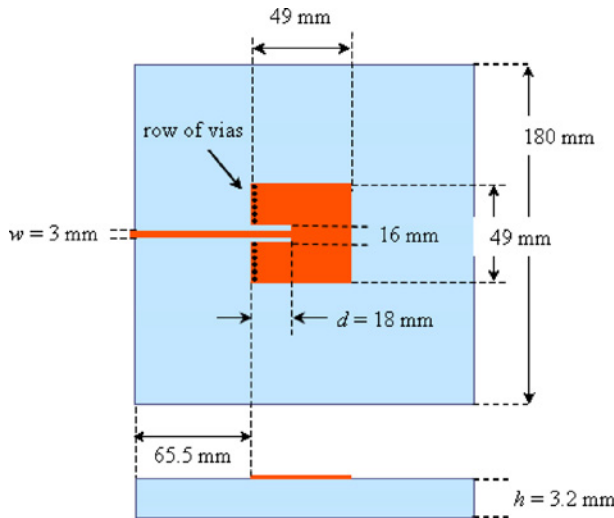


Fig. 5. Dimensions of patch antenna design on magnetic composite substrate (not drawn to scale).

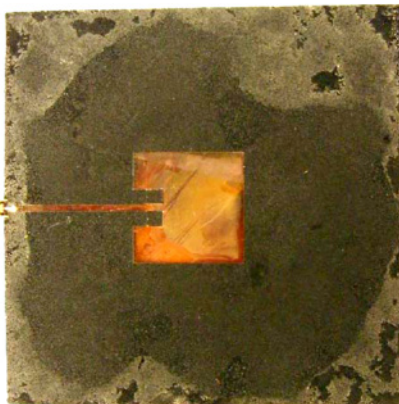


Fig. 6. Photograph of patch antenna prototype on magnetic composite substrate.

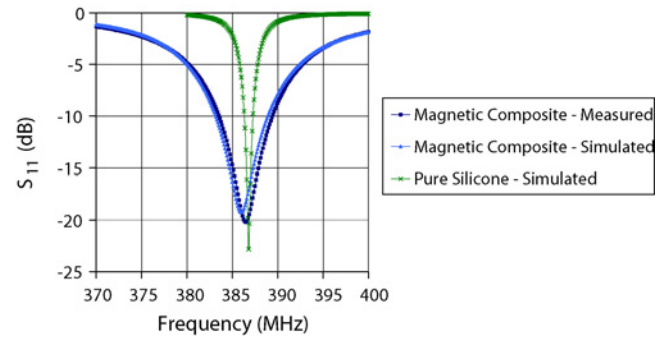


Fig. 7.  $S_{11}$  versus frequency for patch antennas on magnetic composite as measured, magnetic composite as simulated, and pure silicone as simulated.

rotated away from the  $x$ -axis. These figures of merit were obtained by measuring the  $S_{11}$  parameter with a network analyzer and the radiation in an anechoic chamber. For the  $S_{11}$  parameter, the measurement was performed using a Wiltron 37217B Vector Network Analyzer across the frequency range of 300–400 MHz. For the radiation patterns, the measurement was conducted in an anechoic chamber. The gain was obtained using the gain substitution method, by which an adjustable dipole antenna (Scientific Atlanta, Model Number 15–350, Serial Number 264) with fixed 2.0 dBi gain was used as the reference. In both the  $S_{11}$  and radiation pattern measurements, a quarter-wave choke was used to isolate the ground return current on the cable.

#### IV. ANTENNA RESULTS AND DISCUSSION

The  $S_{11}$  parameters obtained for the patch antenna on the magnetic composite as measured and simulated and the pure silicone as simulated are shown in Fig. 7. The 2-D radiation patterns and the adjusted gain at  $\phi = 0^\circ$  and  $90^\circ$  for the patch antenna as simulated on pure silicone and as measured and simulated the magnetic composite are shown in Figs. 8 and 9, respectively. The radiation patterns were taken at the  $f_r$  determined by the  $S_{11}$  parameter for each of the corresponding antenna designs. The antenna performance for the measured magnetic composite antenna, the simulated magnetic composite antenna, and the simulated pure silicone antenna was determined for the figures of merit  $f_r$ ,  $RL$ ,  $-10$  dB  $BW$ , maximum gain, and circuit  $Q$  defined by (2). The summary of antenna performance for all cases is shown in Table III. It should be noted that the measured performance for the pure silicone patch antenna design was not obtained because the maximum required dimensions (i.e., 425 mm square ground, shown in Fig. 4) exceeded the allowable dimensions to prototype with the available fabrication process.

The results of the radiation patterns shown in Figs. 8 and 9 do show a discrepancy for  $\phi = 90^\circ$  for the simulated antenna on the magnetic composite substrate. In this  $\phi = 90^\circ$  measurement, a full back lobe at  $180^\circ$  is shown, whereas it does not exist for both the measured antenna on the magnetic composite substrate and the simulated antenna on the pure silicone substrate. This discrepancy was investigated by simulating the structure in another EM simulation package, Computer

TABLE III  
SUMMARY OF ANTENNA PERFORMANCE

	$f_r$ (MHz)	$RL$ (dB)	$-10$ dB $BW$ (MHz)	Max Gain (dBi)	Circuit $Q$
Magnetic Composite – Measured	386.5	-20.2	5.90	-8.9	66
Magnetic Composite – Simulated	386.0	-19.3	5.74	-9.9	67
Pure Silicone – Simulated	386.8	-22.8	0.96	4.8	403

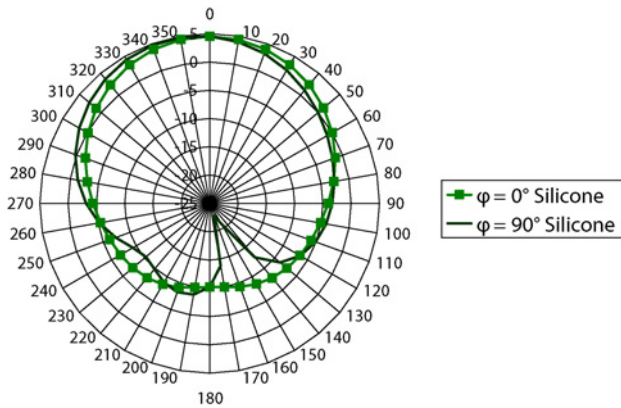


Fig. 8. Radiation pattern and adjusted gain at  $\phi = 0^\circ$  and  $90^\circ$  for patch antenna on silicone as simulated, taken at  $f_r$ .

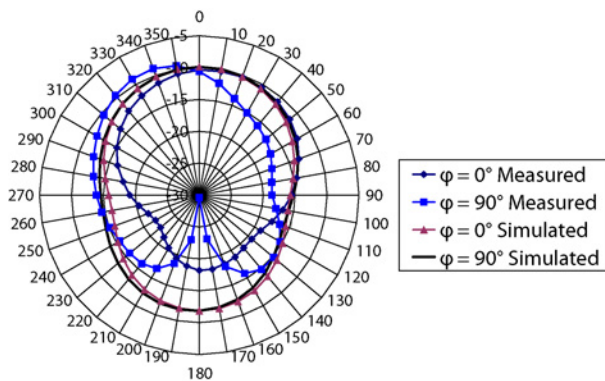


Fig. 9. Radiation pattern and adjusted gain at  $\phi = 0^\circ$  and  $90^\circ$  for patch antenna on magnetic composite as measured and simulated, taken at  $f_r$ .

Simulation Technology Microwave Studio version 2006B.03, which gave the same shape shown here. Additionally, another case was run in Ansoft HFSS for which the product of  $\epsilon_r$  and  $\mu_r$  was inputted as a new  $\epsilon_r$ , while the  $\mu_r$  and  $\tan \delta_\mu$  were set to 1 and 0, respectively ( $\tan \delta_\epsilon$  was left the same) and the same radiation pattern shape shown here was once again obtained. Considering these results and the close agreement between the other simulated and measured results, the discrepancy was attributed to the limitation of the software to model the combined high  $\epsilon_r$  and  $\mu_r$  case.

The close agreement of results for  $f_r$  and  $RL$  for all three cases provides a good foundation on which the other figures of merit can be compared in order to assess differences that may be attributable to the addition of the permeability and magnetic loss. One result that was expected is the increased bandwidth that was obtained for the patch antenna on the magnetic composite substrate due to the addition of magnetic loss.

The maximum gain results for the simulated and measured patch antenna on the magnetic composite substrate are in good agreement. The decrease in the maximum gain for the patch antenna on the magnetic composite substrate compared to the pure silicone substrate may be attributable to both the addition of magnetic loss as well as the decrease in the patch size. For these performance tradeoffs, the capability for miniaturization is demonstrated to be  $2.4\times$  (i.e.,  $425/180\sim 2.4$ ) for applying the developed magnetic composite.

The tradeoff of the antenna performance determined here for the capability of miniaturization can be useful in some applications. Applications that warrant miniaturization, increased bandwidth, and lower maximum gain do exist in or near the lower UHF spectrum. For example, indoor location technology and some other ad hoc networks require high-directivity for device-to-device isolation [13]. Other possible examples include wearable wireless health monitoring and pharmaceutical drug tracking applications that require small size, lightweight conformal antennas.

## V. MATERIAL PROPERTIES SIMULATION STUDY

With the  $2.4\times$  miniaturization capability demonstrated for the patch antenna structure on the flexible magnetic composite substrate, the effects of material properties variation was investigated using a hybrid EM simulation and statistical tools methodology in addition to Monte Carlo simulation.

The hybrid EM simulation and statistical tools methodology used to develop statistical models describing antenna performance as a function of the material properties is presented in Fig. 10. The experimental design chosen for the first-order statistical model was a full factorial design of experiment (DOE) with center points [14]. The  $2^k$  factorial design is the simplest one, with  $k$  factors at 2 levels each. It provides the smallest number of runs for studying  $k$  factors and is widely used in factor screening experiments [14]. Center points are defined at the center of the design space and increase the capability for investigating the validity of the model, including the curvature in the response, while accounting for variation inherent in obtaining the true values of both the factors and responses. As further described by Fig. 10, if the ultimate lack of fit is determined for the models, the analysis is extended to develop second-order models. Developing second-order models requires addition of axial points for response surface methodology (RSM), which can account for the curvature [15]. The second-order models can be reasonable approximations of the true functional relationship over relatively small ranges. Factorial designs have been used in experiments involving several factors where the goal is the study of the joint effects of the factors on a response or responses [16]. To perform the

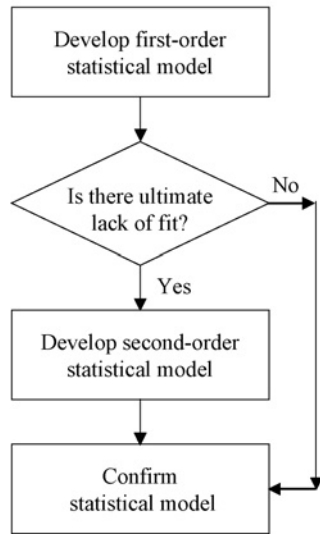


Fig. 10. Methodology for developing statistical models.

statistical analysis required to execute this methodology, JMP software was used [17].

Using the final statistical models, Monte Carlo simulation was applied to investigate the effects of material properties variation on the antenna performance variation. A total of 20 000 trials were performed on the assumed variation of the material properties in order to obtain the simulated variation of the antenna performance. Then, capability analysis was performed to determine whether the simulated antenna performance was capable of  $6\sigma$  performance. Six Sigma capability is reached for processes that have both lower specification limit (LSL) and upper specification limit (USL) and achieve  $C_p > 2.0$  and  $C_{pk} > 1.5$ , realizing no more than 3.4 parts per million opportunities and assuming long-term process shift of  $\pm 1.5$  sigma shift. Six Sigma capability is reached for processes that have either LSL or USL and achieve  $C_{pk} > 1.5$ , realizing no more than 3.4 parts per million opportunities and assuming long-term process shift of  $\pm 1.5$  sigma shift.  $C_{npk}$  is substituted for  $C_{pk}$  when the data is nonnormal. Finally, sensitivity analysis was performed to determine the relative contributions of variation due to the material properties to the variation in antenna performance. Monte Carlo simulation has been used in experiments involving several factors where the goal is the study of the effects of the variation of the factors on the variation of a response or responses [18]. To perform the Monte Carlo simulation and analyses, Crystal Ball software was used [19].

To begin, the antenna figures of merit selected as the output variables, or the experimental responses, were  $f_r$ ,  $RL$  at 386 MHz, and maximum gain at 386 MHz. These figures of merit describe the capability of the antenna to operate at the targeted operating frequency of 386 MHz. Next, the material properties  $\epsilon_r$  and  $\mu_r$  were selected as the input variables, or the experimental factors. These material properties were chosen for the simulated experiment because it was previously observed that  $\epsilon_r$  and  $\mu_r$  for the Co<sub>2</sub>Z ferrite could vary for

TABLE IV  
DOE FOR THE SIMULATED EXPERIMENT

Material Property	Center Point	Low (-)	High (+)
$\epsilon_r$	6	5.91	6.09
$\mu_r$	3	2.955	2.955

different batches, and from experience gained in the work, it was observed that  $\epsilon_r$  and  $\mu_r$  can significantly affect the antenna figures of merit. Because the nominal values at 386 MHz for  $\epsilon_r$  and  $\mu_r$  of 3 and 6, respectively, the previous antenna design on the magnetic composite (Fig. 5) was slightly modified to resonate at the target operating frequency of 386 MHz. The only change in the antenna design was the decrease in the size of the square patch from 49 mm to 44.75 mm in order to accommodate the slight increase in the nominal material property values.

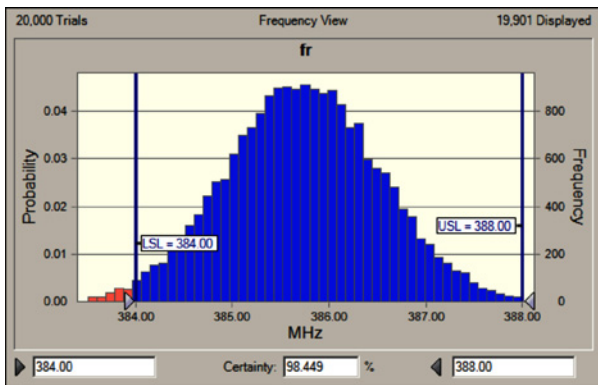
The DOE experimental design is described in Table IV. The  $\pm 1.5\%$  ranges were chosen to minimize the probability of extrapolating beyond the design space that the statistical models describe, when the  $\pm 1.0\%$  tolerances for the material properties were applied for the Monte Carlo simulations. Since the statistical models were based on deterministic simulations, the variation of the center points was based on an assumed  $\pm 0.1\%$  tolerance capability for measuring the material properties. For both the  $\pm 1.0\%$  and  $\pm 0.1\%$  tolerances, a  $3\sigma$  process for  $\epsilon_r$  and  $\mu_r$  was assumed to derive the standard deviations. Because curvature was found in at least one of the responses, axial points were added to the DOE, thereby producing an RSM experimental design.

The final statistical models resulting from this methodology for  $f_r$ ,  $RL$  at 386 MHz, and maximum gain at 386 MHz are given by (3), (4), and (5), respectively. All three models were checked and validated for the assumptions of normality and equal variance of the residuals. The assumption of independence was taken as valid, because the data was obtained deterministically from the EM simulation. Additionally, all three models were confirmed with a new simulated condition of  $\epsilon_r$  and  $\mu_r$  equal to 6.080 and 3.040, respectively, supporting that the models had sufficient capability of predicting.

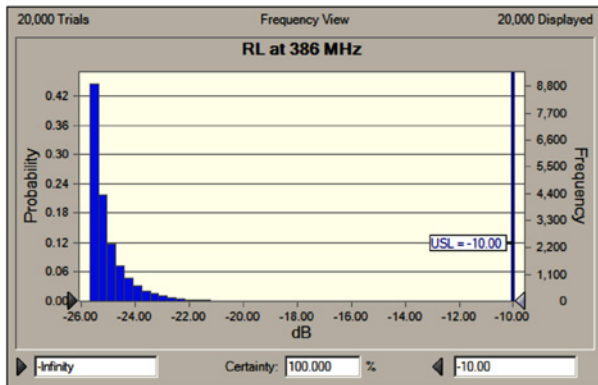
$$f_r = 385.73 - 2.734 \left( \frac{\epsilon' - 6}{0.09} \right) - 2.276 \left( \frac{\mu' - 3}{0.045} \right) \quad (3)$$

$$\begin{aligned} RL \text{ at } 386 \text{ MHz} = & -25.672 + 0.7194 \left( \frac{\epsilon' - 6}{0.09} \right) \\ & + 0.1282 \left( \frac{\mu' - 3}{0.045} \right) + 9.028 \left( \frac{\epsilon' - 6}{0.09} \right) \\ & \times \left( \frac{\mu' - 3}{0.045} \right) + 6.696 \left( \frac{\epsilon' - 6}{0.09} \right)^2 \\ & + 5.878 \left( \frac{\mu' - 3}{0.045} \right)^2 \end{aligned} \quad (4)$$

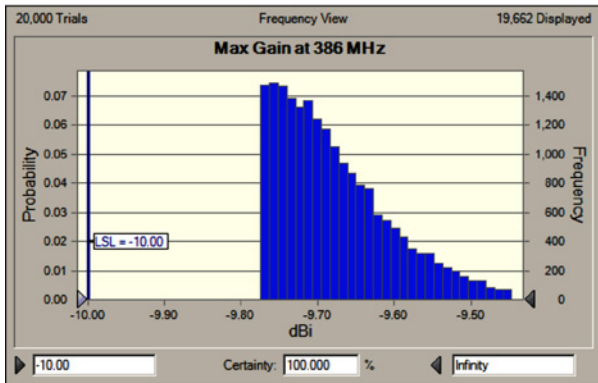
$$\begin{aligned} \text{Max Gain at } 386 \text{ MHz} = & -9.693 - 0.3444 \left( \frac{\epsilon' - 6}{0.09} \right) \\ & + 0.3892 \left( \frac{\epsilon' - 6}{0.09} \right)^2. \end{aligned} \quad (5)$$



(a)



(b)

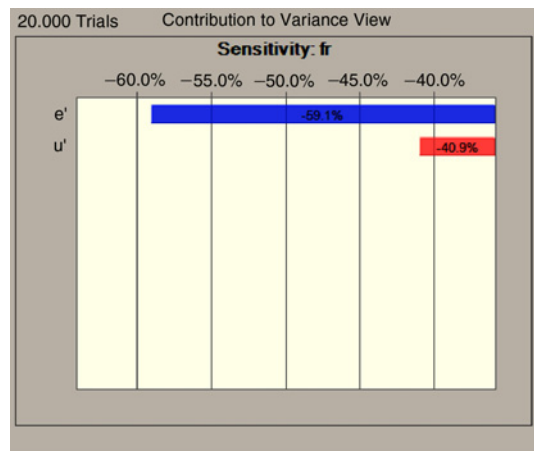


(c)

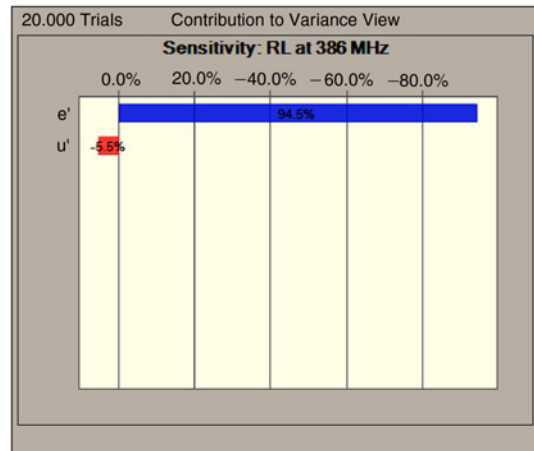
Fig. 11. Distributions resulting from Monte Carlo simulations for antenna performance figures of merit. (a)  $f_r$ . (b)  $RL$  at 386 MHz. (c) Maximum gain at 386 MHz.

Using these final statistical models, Monte Carlo simulation consisting of 20 000 trials was run for  $\epsilon_r$  and  $\mu_r$  in order to obtain the distributions of the antenna performance figures of merit  $f_r$ ,  $RL$  at 386 MHz, and maximum gain at 386 MHz. The resulting distributions are shown in Fig. 11.

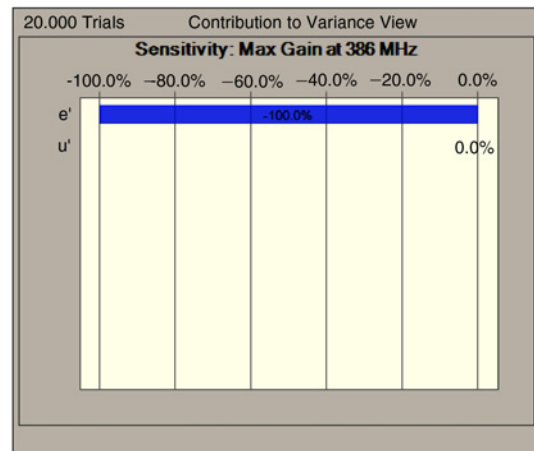
Capability analysis was performed on these results to determine whether  $f_r$ ,  $RL$  at 386 MHz, and maximum gain at 386 MHz were capable of  $6\sigma$  performance. The quantities for  $C_p$ ,  $C_{pk}$ , and  $C_{npk}$  can be used to assess  $6\sigma$  capability. Six Sigma capability is reached for processes that achieve  $C_p > 2$  and  $C_{pk} > 1.5$  for processes with USL and LSL, and  $C_{pk}$  or  $C_{npk} > 1.5$  for processes with only USL or LSL, allowing in both cases the possibility of long-term  $\pm 1.5$  sigma shift.



(a)



(b)



(c)

Fig. 12. Sensitivity analysis resulting from Monte Carlo simulations for antenna performance figures of merit. (a)  $f_r$ . (b)  $RL$  at 386 MHz. (c) Maximum gain at 386 MHz.

In other words, the designer knows at the beginning of the design process that, with  $6\sigma$  performance, approximately 3.4 measurements out of 1 000 000 may occur beyond these specification limits (i.e., the USL and LSL). If the designer finds performance less than  $6\sigma$  unacceptable, the whole system can be redesigned, again through simulation, without the need to build any test structures and go through an expensive, time

TABLE V  
SUMMARY OF CAPABILITY ANALYSIS RESULTS

Process Information	$f_r$	RL at 386 MHz	Max Gain at 386 MHz
Target	386 MHz	not applicable	Not applicable
LSL	384 MHz	not applicable	-10 dBi
USL	388 MHz	-10 dB	not applicable
$C_p$	0.84	not applicable	not applicable
$C_{pk}$	0.73	not applicable	not applicable
$C_{npk}$	not applicable	3.74	3.88

consuming full design cycle. As part of the capability analysis, the distributions were tested to determine if they were normally distributed. At the 95% confidence level,  $f_r$  was found to be normally distributed, whereas RL at 386 MHz and maximum gain at 386 MHz were not normally distributed. In the cases of RL at 386 MHz and maximum gain at 386 MHz,  $C_{npk}$  was used because the normality assumption was not verified. Results of the capability analysis showed  $f_r$  not to be  $6\sigma$  capable for the assumed specification limits, because  $C_p$  and  $C_{pk}$  were found to be less than 2.0 and 1.5, respectively. Both RL at 386 MHz and maximum gain at 386 MHz were determined to be  $6\sigma$  capable for the assumed specification limits, because the  $C_{npk}$  values were found to be greater than 1.5. The summary of the capability analysis results is shown in Table V.

The sensitivity analysis was performed to determine the relative contributions of the variation due to  $\epsilon_r$  and  $\mu_r$  to the variation in  $f_r$ , RL at 386 MHz, and maximum gain at 386 MHz. The resulting sensitivity analysis is shown in Fig. 12. It was found that the variation of  $\epsilon_r$  contributed more than  $\mu_r$  to the variation in the antenna performance. The inputs  $\epsilon_r$  and  $\mu_r$  contributed 59.1% and 40.9%, respectively, to the variation in  $f_r$ , and 94.5% and 5.5%, respectively, to the variation in RL at 386 MHz. Only  $\epsilon_r$  contributed to the variation in maximum gain at 386 MHz, which was expected since the model developed for maximum gain at 386 MHz included the dependence on  $\epsilon_r$  alone. Based on these results, controlling the variation of  $\epsilon_r$  provides a large opportunity for controlling variation of  $f_r$ , RL at 386 MHz, and maximum gain at 386 MHz.

## VI. EFFECT OF DIELECTRIC AND MAGNETIC LOSSES

The effect of dielectric and magnetic losses on antenna performance was investigated by comparing EM simulation results of the antenna designs assuming actual  $\tan \delta_\epsilon$  and  $\tan \delta_\mu$  values and these values set equal to zero. The first EM simulation was performed at the center point for the RSM, which was  $\epsilon_r$  and  $\mu_r$  equal to 6 and 3, respectively, for the original antenna design used in the material properties variation study. A poor RL was obtained and attributed to the change in characteristic impedance  $Z_0$ , which was no longer equal to  $50 \Omega$  and thereby caused reflection of the input power. A retuned design was achieved by adjusting only  $w$  and  $d$  equal to 1.0 mm and 1.4 mm, respectively, thereby not affecting the patch or overall antenna size. Then, a second EM simulation was performed with the retuned design assuming  $\tan \delta_\epsilon$  and  $\tan \delta_\mu$  both equal to zero. To investigate effect of the

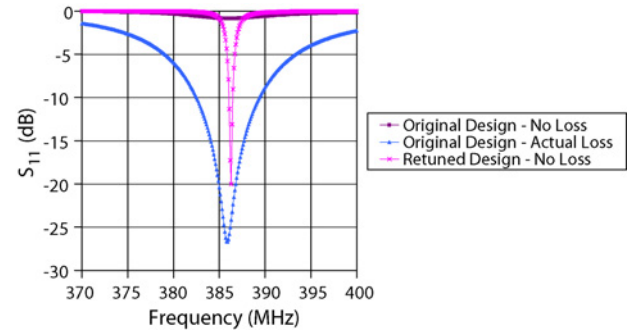


Fig. 13.  $S_{11}$  versus frequency to investigate effect of dielectric and magnetic losses.

losses, the antenna figures of merit  $f_r$ , RL at 386 MHz, and maximum gain at 386 MHz were compared for the original design with no loss, the original design with actual loss, and the retuned design with no loss.

To compare  $f_r$  and RL at 386 MHz for these cases, the  $S_{11}$  versus frequency is shown in Fig. 13. The dielectric and magnetic losses slightly affected  $f_r$ , with values of 385.9, 385.9, and 386.3 MHz for the patch antenna on magnetic composite assuming the original design with no loss, the original design with actual loss, and the retuned design with no loss, respectively. The loss did affect RL at 386 MHz, as the values of  $-0.8472$ ,  $-26.4044$ , and  $-7.9137$  for the patch antenna on magnetic composite assuming the original design with no loss, the original design with actual loss, and the retuned design with no loss, respectively, were substantially different. For the retuned design, only limited RL at 386 MHz was achieved, which was attributed to the slight change in  $f_r$  and the comparatively narrower BW.

The values of maximum gain at 386 MHz were considered for these cases as well as for the pure silicone case. The dielectric and magnetic losses were found to also affect maximum gain at 386 MHz, as observed when the values of 3.7,  $-9.7$ , 3.6, and 4.8 dBi were compared for the patch antenna on magnetic composite assuming the original design with no loss, the original design with actual loss, the retuned design with no loss, and the previous design on pure silicone shown in Fig. 4, respectively. It was noted that the values of maximum gain at 386 MHz that were obtained from the simulation did not include effects of the microstrip impedance matching. Considering the differences in the values for maximum gain at 386 MHz, the decrease in the maximum gain for the patch antenna on the magnetic composite substrate compared to the pure silicone substrate may be attributable to

both the addition of the dielectric and magnetic losses as well as the decrease in the patch size.

## VII. CONCLUSION

The capability of miniaturization by a factor of  $2.4\times$  was demonstrated for a patch antenna structure on a mechanically flexible magnetic composite substrate when compared to a pure silicone substrate. Differences in performance of the antennas included increased bandwidth and reduced gain, both of which were attributed in part to the increase in the dielectric and magnetic losses. These differences can be either beneficial or detrimental, depending on the design motivation, and, in effect, provide further flexibility in radio frequency (RF) system design. A key finding of this paper was that a small amount of permeability ( $\mu_r \sim 2.5$ ) can provide relatively substantial capability for miniaturization, while sufficiently low-magnetic loss can be introduced for successful application at the targeted operating frequency. This magnetic composite shows the capability to fulfill this balance and to be a feasible option for RFID applications in the lower UHF spectrum ( $\sim 300$ – $500$  MHz). Another key finding was that controlling the variation of  $\epsilon_r$  provides a large opportunity for controlling variation of  $f_r$ ,  $RL$  at 386 MHz, and maximum gain at 386 MHz.

## ACKNOWLEDGMENT

The authors would like to thank B. W. Treadway of Trans-Tech in Adamstown, Maryland, and D. J. Meyer of Motorola in Plantation, Florida, for their support of this paper.

## REFERENCES

- [1] D. Dressen, "Large memory RFID system solutions," *Atmel Appl. J.* pp. 48–49 [Online]. Available: [http://www.atmel.com/dyn/resources/prod\\_documents/secrref\\_largemem\\_3\\_04.pdf](http://www.atmel.com/dyn/resources/prod_documents/secrref_largemem_3_04.pdf)
- [2] *Magnetic Materials for RFID*, TechnoForum, TDK, Tokyo, Japan, 2005 [Online]. Available: [http://www.tdk.co.jp/tf2005/pdf\\_e/2f0215e.pdf](http://www.tdk.co.jp/tf2005/pdf_e/2f0215e.pdf)
- [3] J. Masi and W. Thibault, "New, high frequency transformer topologies," in *Proc. Electr. Electron. Insul. Conf. Elect. Manuf. Coil Wind. Conf.*, Rosemont, IL, Sep. 1995, pp. 157–161.
- [4] N. Das and A. K. Ray, "Magneto optical technique for beam steering by ferrite based patch arrays," *IEEE Trans. Antennas Propag.*, vol. 49, no. 8, pp. 1239–1241, Aug. 2001.
- [5] W. A. Roshen, C. S. Korman, and W. Daum, "Embedded magnetics for integrated power," in *Proc. 35th Annu. IEEE Power Electron. Specialists Conf.*, Aachen, Germany, Jun. 2004, pp. 2467–2473.
- [6] S. Das and S. Chowdhury, "Rectangular microstrip antenna on a ferrite substrate," *IEEE Trans. Antennas Propag.*, vol. 30, no. 3, pp. 499–502, May 1982.
- [7] J. Yeo, R. Mitra, and S. Chakravarty, "A GA-based design of electromagnetic bandgap (EBG) structures utilizing frequency selective surfaces for bandwidth enhancement of microstrip antennas," in *Proc. IEEE Int. Antennas Propag. Symp.*, San Antonio, TX, Jun. 2002, pp. 400–403.
- [8] J. Yeo, J.-F. Ma, and R. Mitra, "Design of artificial magnetic ground planes (AMGs) utilizing frequency selective surfaces embedded in multilayer structures with electric and magnetic losses," in *Proc. IEEE Int. Antennas Propag. Symp.*, Columbus, OH, Jun. 2003, pp. 343–346.
- [9] A. B. Smolders, "Broadband microstrip array antennas," in *Proc. IEEE Int. Antennas Propag. Symp.*, Seattle, WA, Jun. 1994, pp. 1832–1835.
- [10] N. P. Mahalik, "Tuning procedure in microstrip antennas on ferrite substrate," in *Proc. IEEE Int. Antennas Propag. Symp.*, vol. 1. Edinburgh, U.K., Apr. 1997, pp. 294–297.

- [11] G. H. Jonker, H. P. J. Wijn, and P. B. Braun, "Ferroplana, hexagonal ferromagnetic iron-oxide compounds for very high frequencies," *Philips Tech. Rev.*, vol. 18, no. 6, pp. 145–154, 1956–1957.
- [12] H. Zhang, L. Li, J. Zhou, Z. Yue, and X. Gui, "Dielectric characteristics of Cu modified Z-type plana hexaferrite," in *Proc. IEEE 12th Int. Symp. Appl. Ferroelectr.*, vol. 2. Honolulu, HI, Jul.–Aug. 2000, pp. 859–862.
- [13] G. Jakllari, I. Broustis, T. Korakis, S. V. Krishnamurthy, and L. Tassiulas, "Handling asymmetry in gain in directional antenna equipped ad hoc networks," in *Proc. IEEE 16th Int. Symp. Personal, Indoor Mobile Radio Commun.*, Berlin, Germany, Sep. 2005, pp. 1284–1288.
- [14] G. E. P. Box, W. G. Hunter, and J. S. Hunter, in *Statistics for Experimenters: An Introduction to Design, Data Analysis, and Model Building*, New York: John Wiley, 1978.
- [15] J. Neter, M. H. Kutner, C. J. Nachtsheim, and W. Wasserman, in *Applied Linear Statistical Models*, 4th ed. Chicago: McGraw-Hill, 1996.
- [16] C. You, D. Staiculescu, L. J. Martin, and M. M. Tentzeris, "A novel hybrid electrical/mechanical optimization technique using time-domain modeling, finite element method and statistical tools for the co-design and optimization of RF integrated mechanical structures," *Int. J. Numer. Model.*, vol. 21, nos. 1–2, pp. 91–101, Jan. 2008.
- [17] *JMP Software*, Version 6.0.3, Cary, NC: SAS Institute, 2006.
- [18] D. Staiculescu, L. J. Martin, and M. M. Tentzeris, "Performance capability modeling and optimization of RF/millimeter wave integrated functions and modules using a hybrid statistical/electromagnetic technique that includes process variations," in *Proc. 36th Eur. Microw. Conf.*, Manchester, U.K., Sep. 2006, pp. 474–477.
- [19] *Crystal Ball Software*, Version 7.3, Denver, CO: Decisioneering, Apr. 2007.



**Lara J. Martin** (M'98) received the Bachelor degree in chemical engineering, the M.S. degree in materials science and engineering, and the Ph.D. degree in materials science and engineering with a minor in applied statistics, from the Georgia Institute of Technology, Atlanta, in 1995, 2000, and 2008, respectively.

She has used her background in both engineering and statistics throughout her career at Motorola, Plantation, FL, where she currently works as a Master Black Belt for Motorola's Enterprise Mobility Solutions. She achieved a Six Sigma Black Belt in 2001 and became the 17th Master Black Belt recognized in Motorola in 2003, for her application of statistical tools and methods. She has published 32 papers in several forums, including conference proceedings, peer-reviewed journals, and a cover story article for a trade magazine. She holds several U.S. and international patents.

Dr. Martin was inducted as a Motorola Science Advisory Board Associate Member in 2003, representing the top 1.5% of the corporation's technical resources. Additionally, she was elected to the Georgia Tech Council of Outstanding Young Engineering Alumni in 2004 and was awarded the IEEE Components, Packaging, and Manufacturing Technology Outstanding Young Engineer of the Year Award in 2005.



**Sooliam Ooi** (SM'89) received the B.S. degree from the University of Technology Malaysia, Skudai, Johor, in 1988, the M.S. degree from the University of Malaya, Kuala Lumpur, in 1996, and the Ph.D. degree from Malaysia Multimedia University, Cyberjaya, in 2005, all in electrical engineering.

He joined the Antenna Innovation Labs for Motorola Mobile Devices, Libertyville, IL, as a Distinguished Member of Technical Staff in 2008. He joined Research in Motion, Sunrise, FL, in 2009, and currently serves as a Senior Antenna Designer for Blackberry Research and Development. He served as a Distinguished Member of the Technical Staff for Motorola Corporate Research Labs from 2000 to 2008. He conducted in-depth research on multipitch helical antenna technology for multiband applications, filed two patents on the concepts, and adopted the design for the Motorola. He engineered portable radio antennas for major Motorola portable radio products from 1992 to 2007. His research interests include handset antenna design for public safety bands, and cellular bands.



**Daniela Staiculescu** (M'97) received the B.S. degree in electrical engineering from the Polytechnic University, Bucharest, Romania, in 1993, and the M.S. and Ph.D. degrees in electrical and computer engineering from Georgia Institute of Technology, Atlanta, in 1999 and 2001, respectively.

From 2001 to 2003, she was a Senior Design Engineer with Radio Frequency Solutions, Atlanta, GA, and she is currently a Senior Research Engineer in the Athena Group at the Georgia Institute of Technology, Atlanta. She uses statistical techniques,

like design of experiments and response surface modeling, for design rule development/optimization, and for analysis of passive systems. She has authored 50 papers, filed one invention disclosure, and co-authored two book chapters. She is actively involved in international student exchange programs. Her research interests include wireless sensor networks for various applications like body area networks, automotive, power scavengers, and structure health monitoring. She is also interested in new materials, like link control protocol, paper electronics, magnetic composites, and nanotechnology.

Dr. Staiculescu is a Reviewer for several IEEE journals. She is a Member of the International Microwave Symposium Transaction Processing Performance Council, and is involved in the Steering Committees of several IEEE conferences and workshops.



**Michael D. Hill** received the B.S. degree in materials engineering and the M.S. degree in materials science and engineering from Virginia Polytechnic Institute and State University, Blacksburg, in 1986 and 1988, respectively. He received the Ph.D. degree in materials science and engineering from the University of Maryland, College Park, in 1996.

From 1989 to 1996, he was a Ceramic Engineer with the National Institute of Standards and Technology, Gaithersburg, MD. He works on and has published papers on crystal chemistry of high  $T_c$

superconductors, and synthesis of lead-based Perovskites. He has been with the Department of Research and Development, Trans-Tech, Adamstown, MD, since 1996, where he works on new formulations for microwave dielectric and magnetic materials as well as specialty advanced materials, and helps develop several new formulations. His research interests include crystal chemistry and ceramic processing of microwave dielectric and magnetic oxide materials, as well as crystal chemistry and processing of oxide materials for energy applications.



**C. P. Wong** (F'92) received the B.S. degree in chemistry from Purdue University, West Lafayette, IN, and the Ph.D. degree in chemistry from Pennsylvania State University, University Park.

He is a Regents' Professor and the Charles Smithgall Institute Endowed Chair at the School of Materials Science and Engineering, Georgia Institute of Technology (GT), Atlanta. Prior to joining GT in 1996, he was with AT&T Bell Laboratories, Murray Hill, NJ, for many years, and became an AT&T Bell Laboratories Fellow in 1992. After his doctoral

study, he was awarded a two-year postdoctoral fellowship with Nobel Laureate Professor Henry Taube, Stanford University, Stanford, CA. He holds over 50 U.S. patents, has published over 900 technical papers, and has co-authored and edited ten books. His research interests include polymeric electronic materials, electronic, photonic and microelectro-mechanical system packaging and interconnect, interfacial adhesions, nano-functional and material syntheses and characterizations, nano-composites such as well-aligned carbon nanotubes, grahenes, lead-free alloys, flip chip underfill, ultrahigh k capacitor composites, and novel lotus effect coating materials.

Dr. Wong has received many awards, including the AT&T Bell Labs Fellow Award in 1992, the IEEE Components, Packaging, and Manufacturing Technology Society Outstanding Sustained Technical Contributions Award in 1995, the IEEE Third Millennium Medal in 2000, the IEEE Educational Activities Board Award in 2001, the IEEE Components, Packaging, and Manufacturing Technology Society Exceptional Technical Contributions Award in 2002, the Georgia Tech Class 1934 Distinguished Professor Award in 2004, Named Holder of the Charles Smithgall Chair (one of the two Grounded Theory Institute Chairs) in 2005, the Grounded Theory Outstanding Ph.D. Thesis Advisor Award, the IEEE Components, Packaging, and Manufacturing

Technology Field Award in 2006, the Sigma Xi's Monie Ferst Award in 2007, the Society of Manufacturing Engineers' Total Excellence in Electronic Manufacturing Award in 2008, and the IEEE COMPONENTS, PACKAGING, AND MANUFACTURING TECHNOLOGY David Feldman Award in 2009. He has been a Member of the National Academy of Engineering since 2000.



**Manos M. Tentzeris** (SM'02) received the Diploma degree (magna cum laude) in electrical and computer engineering from the National Technical University of Athens, Athens, Greece, in 1992, and the M.S. and Ph.D. degrees in electrical engineering and computer science from the University of Michigan, Ann Arbor, in 1994 and 1998, respectively.

He is currently a Professor with the School of Electrical and Computer Engineering, Georgia Institute of Technology, Atlanta. He heads the Athena Research Group, and he was a Visiting Professor

with the Technical University of Munich, Munich, Germany, for the summer of 2002, where he introduced a course in the area of high-frequency packaging. He is the Georgia Electronic Design Center Associate Director for RFID/Sensors research, and he has been the Georgia Tech National Science Foundation (NSF)-Packaging Research Center Associate Director for RF Research, and the RF Alliance Leader from 2003 to 2006. He has published more than 320 papers in refereed journals and conference proceedings, three books, and 17 book chapters. He has helped to develop academic programs in highly integrated/multilayer packaging for radio frequency (RF) and wireless applications using ceramic and organic flexible materials, paper-based radio frequency identifications (RFID) and sensors, microwave MEMS, standard operating procedure-integrated ultrawideband, multiband, conformal antennas and adaptive numerical electromagnetics (finite-difference time-domain, MultiResolution algorithms), and "green" RF electronics. He has given more than 50 invited talks in the same area to various universities and companies in Europe, Asia, and America.

Dr. Tentzeris was the recipient or co-recipient of the 2007 IEEE Antennas and Propagation Society (APS) Symposium Best Student Paper Award, the 2007 IEEE International Microwave Symposium (IMS) Third Best Student Paper Award, the 2007 International Symposium on Antennas and Propagation 2007 Poster Presentation Award, the 2006 IEEE Microwave Theory and Techniques (MTT) Outstanding Young Engineer Award, the 2006 Asian-Pacific Microwave Conference Award, the 2004 IEEE Transactions on Advanced Packaging Commendable Paper Award, the 2003 National Aeronautics and Space Administration Godfrey "Art" Anzic Collaborative Distinguished Publication Award, the 2003 International Biographical Center International Educator of the Year Award, the 2003 IEEE Components, Packaging, and Manufacturing Technology (CPMT) Outstanding Young Engineer Award, the 2002 International Conference on Microwave and Millimeter-Wave Technology Best Paper Award, the 2002 Georgia Tech-ECE Outstanding Junior Faculty Award, the 2001 Association for Counselor Education and Supervision Conference Best Paper Award, the 2000 NSF CAREER Award, and the 1997 Best Paper Award of the International Hybrid Microelectronics and Packaging Society. He was the Technical Program Committee Chair for the IEEE IMS 2008 Symposium, and the Chair of the 2005 IEEE Computational Electromagnetics in Time-Domain Workshop. He is the Vice-Chair of the RF Technical Committee (TC16) of the IEEE CPMT Society, the Founder and Chair of the RFID Technical Committee (TC24) of the IEEE MTT Society, and the Secretary/Treasurer of the IEEE C-RFID. He has organized various sessions and workshops on RF/Wireless Packaging and Integration, RFIDs, Numerical Techniques/Wavelets, in the IEEE Electronic Components and Technology Conference, IMS, Virtual Training Center, and APS Symposia in all of which he is a Member of the Technical Program Committee in the area of "Components and RF." He is an Associate Editor of IEEE TRANSACTIONS ON MICROWAVE THEORY AND TECHNIQUES, IEEE TRANSACTIONS ON ADVANCED PACKAGING, and the *International Journal on Antennas and Propagation*. He is a Member of URSI-Commission D, a Member of the MTT-15 committee, an Associate Member of the European Microwave Association, a Fellow of the Electromagnetic Academy, and a Member of the Technical Chamber of Greece. He was the recipient of the 2009 E.T.S.Walton Award from the Irish Science Foundation and he will be the IEEE MTT-S Distinguished Microwave Lecturer from 2010-2012.